

**Influence of Grain Boundary Migration on {001} Texture Formation
in Al-3 mass%Mg Based Alloys during High Temperature
Compression Deformation**

Kazuto Okayasu, Hiroki Takekoshi and Hiroshi Fukutomi

Reprinted from

MATERIALS TRANSACTIONS, VOL. 48 NO. 8, AUGUST, 2007

THE JAPAN INSTITUTE OF METALS

1-14-32, Ichibancho, Aoba-ku, Sendai 980-8544, Japan

Influence of Grain Boundary Migration on {001} Texture Formation in Al-3 mass%Mg Based Alloys during High Temperature Compression Deformation

Kazuto Okayasu, Hiroki Takekoshi* and Hiroshi Fukutomi

Division of Materials Science and Engineering, Graduate School of Yokohama National University, Yokohama 240-8501, Japan

Uniaxial compression tests were conducted on Al-3 mass%Mg alloy and Al-3 mass%Mg-0.2 mass%Sc alloy under various amounts of strain and strain rate at 723 K. High temperature yielding phenomena were observed at 723 K and strain rates ranging from $1.0 \times 10^{-4} \text{ s}^{-1}$ to $5.0 \times 10^{-3} \text{ s}^{-1}$. Texture examination elucidated that fiber textures were constructed in all the deformation conditions. Texture measurement revealed that the main component of the fiber texture changed from {011} + {001} to {001} with an increase in strain when the viscous motion of dislocation is the dominant deformation mechanism in the binary alloy. Texture changes are also seen at strength of the {001} component in the binary alloy that increased with increase in strain rates between $5.0 \times 10^{-4} \text{ s}^{-1}$ and $5.0 \times 10^{-3} \text{ s}^{-1}$ up to a strain of -1.0, while in the ternary alloy, neither variation of the pole density at (011) nor (001) in inverse pole figure is observed in the same deformation conditions. It is considered that Al_3Sc precipitates contribute to the suppression of grain boundary migration. This means that the grain boundary migration contribute to the development of {001} fiber texture. [doi:10.2320/matertrans.L-MRA2007869]

(Received February 1, 2007; Accepted June 5, 2007; Published July 25, 2007)

Keywords: texture, grain boundary migration, scandium trialuminide precipitates, solute atmosphere, electron back-scattered diffraction, high temperature deformation

1. Introduction

The use of aluminum alloys is expected to increase since the automotive lightening is one of the major subjects for resource saving. However, the press formability of aluminum sheet is insufficient compared to that of mild steel. Texture control is a promising method to improve the formability. The texture varies depending on deformation mode, deformation mechanism and heat treatment. Therefore, the understanding of the interrelationship among these factors is important to develop the method to control textures.

In solid solution hardening type Al-Mg alloy, a high temperature yielding phenomenon¹⁾ is observed at high temperatures and certain strain rate. It is known that the high temperature yielding is attributed to the dislocation motion with the Cottrell atmosphere.²⁾

The authors^{3,4)} have been investigated the behaviors of compression deformation and texture formation in an Al-3 mass%Mg solid solution at high temperatures. Texture measurement revealed that the main component of the fiber texture changed from {011} (compression plane) to {011} + {001} and to {001} with an increase in strain when the viscous motion of dislocation is the dominant mechanism of the deformation. It is suggested that the grain boundary migration contributes to the formation of {001} fiber texture.

In this study, behaviors of texture formation in both single phase Al-3 mass%Mg and Al-3 mass%Mg-0.2 mass%Sc with Al_3Sc precipitates which are stable at high temperatures were experimentally investigated at 723 K under various amounts of strain and strain rates, in order to elucidate the role of grain boundary migration in the formation of {001} texture.

2. Experimental Procedure

2.1 Materials and compression tests

The ingot of Al-3 mass%Mg (hereafter expressed as Al-3Mg) alloy was prepared by melting and casting in air. The surface layers of the ingots were removed by machining. After the homogenization, the ingot was rolled to 50% of their original thickness at room temperature. The ingot of Al-3 mass%Mg-0.2 mass%Sc (hereafter expressed as Al-3Mg-0.2Sc) alloy was kindly provided by Kobe Steel, Ltd. in the form of 30% cold rolled plate. After dividing into small pieces, they were additionally rolled to 50% reduction at room temperature. In total, about 68% reduction of their original thickness was given by cold rolling. The chemical compositions (in mass%) of these alloys are shown in Table 1.

Cylindrical specimens with various sizes were prepared by spark erosion machining for compression tests. Aspect ratio of specimens was kept at 1.5 for all sizes of specimens. The specimens of Al-3Mg alloy were annealed at 773 K for 1.2 h before the tests. The specimens of Al-3Mg-0.2Sc alloy were solution treated at 873 K for 1 h and were water quenched. In order to precipitate Al_3Sc , the specimens were aged at 773 K for 49 h and were quenched into water before the tests.

Compression tests were conducted under constant cross-head speed conditions at 723 K in air. Final strain rates were evaluated by the calculation based on the crosshead speed and final height of specimens. In this paper, the final strain

Table 1 Chemical compositions of the alloys (mass%).

Alloy	Mg	Si	Fe	Zn	Al
Al-3Mg	3.32	0.06	0.01	—	bal.
Al-3Mg-0.2Sc	3.10	0.03	0.04	0.01	bal.

*Graduate Student, Yokohama National University. Present address: Hino Motors Ltd., Hino 191-8660, Japan

rate is used to express the deformation condition. Final strain rates were in a range between $1.0 \times 10^{-4} \text{ s}^{-1}$ and $5.0 \times 10^{-3} \text{ s}^{-1}$. The infrared-ray furnace was used for heating. Immediately after the deformation, the furnace was opened and the power supply was switched off simultaneously, and then specimens were quenched into water within at most 20 s, in order to prevent the change in microstructure after high temperature compression test.

2.2 Microstructure observation and texture measurement

After the compression tests, the mid-plane section of the specimens were prepared by mechanical and electrolytic polishing. Microstructures were observed using optical microscope (OM) and scanning electron microscope (SEM). Texture measurements were conducted on the mid-plane sections by the Schulz reflection method using nickel filtered copper $K\alpha$ radiation. The diffracted X-ray intensities were measured on 111, 200 and 220 reflections and $\{111\}$, $\{001\}$ and $\{011\}$ pole figures were constructed. Based on these three pole figures, orientation distribution function (ODF) was calculated by the Dahms-Bunge method.⁵⁾ Textures were examined on the basis of pole figures and inverse pole figures calculated from ODF.

2.3 Grain structure map

Local crystal orientations were measured by the electron back-scattered diffraction (EBSD) technique. The measurements were performed every $4 \mu\text{m}$. The minimum rotation angle θ between neighboring points of measurement was calculated by the commercial program (OIM Analysis Version 3.08) developed by TexSEM Laboratories, Inc. When θ is between 5° and 15° , it is defined as a low angle grain boundary. When θ is larger than 15° , it is defined as a high angle grain boundary. Figures on the position and the shape of grains were drawn based on the orientation measurement. These figures are expressed "grain structure maps" in the present paper.

3. Results

3.1 Initial microstructures

Figures 1(a)(b) and (c) show OM and SEM micrographs before compression, respectively. Figure 1(a) exhibits for Al-3Mg, Figs. 1(b) and (c) for Al-3Mg-0.2Sc. Figure 1(c) was taken using backscattered electron mode. Many Al_3Sc precipitates smaller than $1 \mu\text{m}$ are observed in grains, while large particles, probably Al_3Sc , exist along the grain boundaries as white particles. The average grain sizes of these Al-3Mg and Al-3Mg-0.2Sc alloys derived from OM micrographs using linear intercept method are $90 \mu\text{m}$ and $99 \mu\text{m}$, respectively. These two alloys consist of equiaxed grains, and grain orientations were confirmed to be random.

3.2 Stress – Strain Curves

Figure 2 shows the true stress - true strain curves examined at 723 K under strain rates of $1.0 \times 10^{-4} \text{ s}^{-1}$, $1.0 \times 10^{-3} \text{ s}^{-1}$ and $5.0 \times 10^{-3} \text{ s}^{-1}$. Figures 2(a) and (b) exhibit the results of Al-3Mg and Al-3Mg-0.2Sc, respectively. The high temperature yielding phenomena are observed in all the cases. Flow

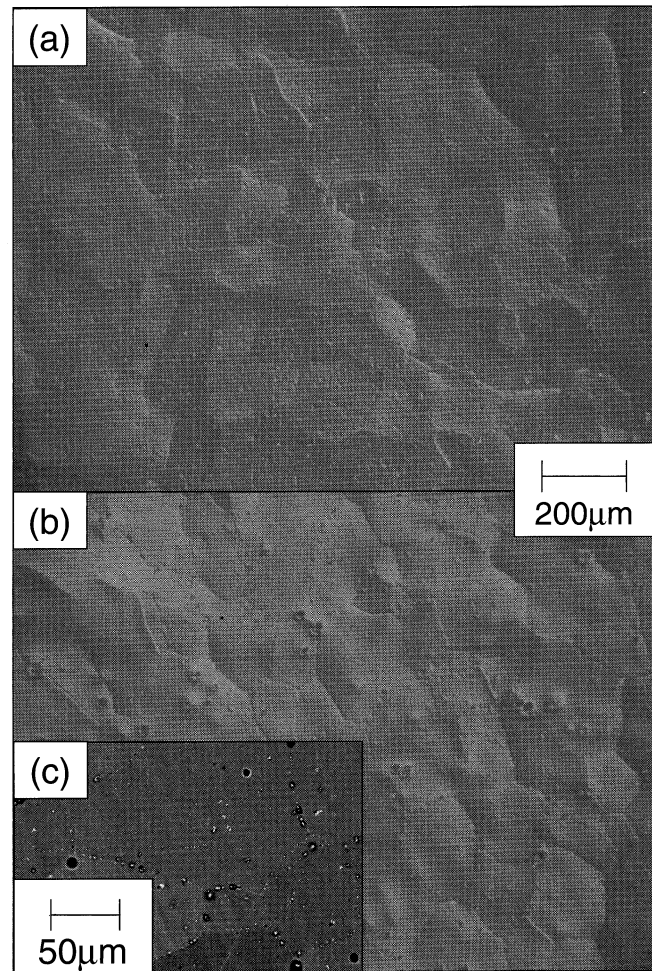


Fig. 1 Optical micrographs and backscattered electron micrograph before compression. (a) shows the microstructure of Al-3Mg. (b) and (c) show the microstructures of Al-3Mg-0.2Sc. Al_3Sc precipitates are shown in (c) as white particles.

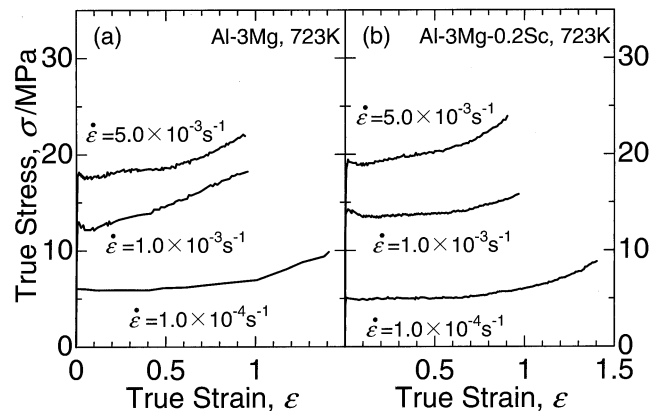


Fig. 2 True stress – true strain curves obtained by compression test at 723 K under final strain rates of $5.0 \times 10^{-3} \text{ s}^{-1}$, $1.0 \times 10^{-3} \text{ s}^{-1}$ and $1.0 \times 10^{-4} \text{ s}^{-1}$. (a) and (b) show the results of Al-3Mg and Al-3Mg-0.2Sc, respectively.

stresses decrease with decrease in strain rate. The level of flow stress of Al-3Mg-0.2Sc shown in Fig. 2(b) is less than half of that reported by Ihara and Miura⁶⁾ where the aging was conducted at 723 K (50 K lower than the present case) for 10^5 s (about one half of the present case). The stress-strain

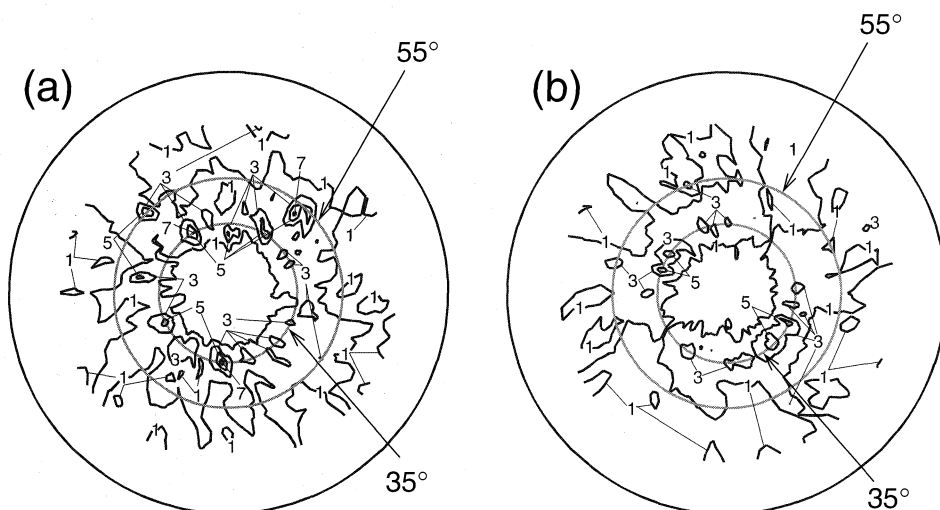


Fig. 3 {111} pole figures for the specimens of (a) Al-3Mg and (b) Al-3Mg-0.2Sc compressed at 723 K under a final strain rate of $1.0 \times 10^{-3} \text{ s}^{-1}$ up to a strain of -1.0 . The pole density is projected onto the compression plane. The average pole density is used as units.

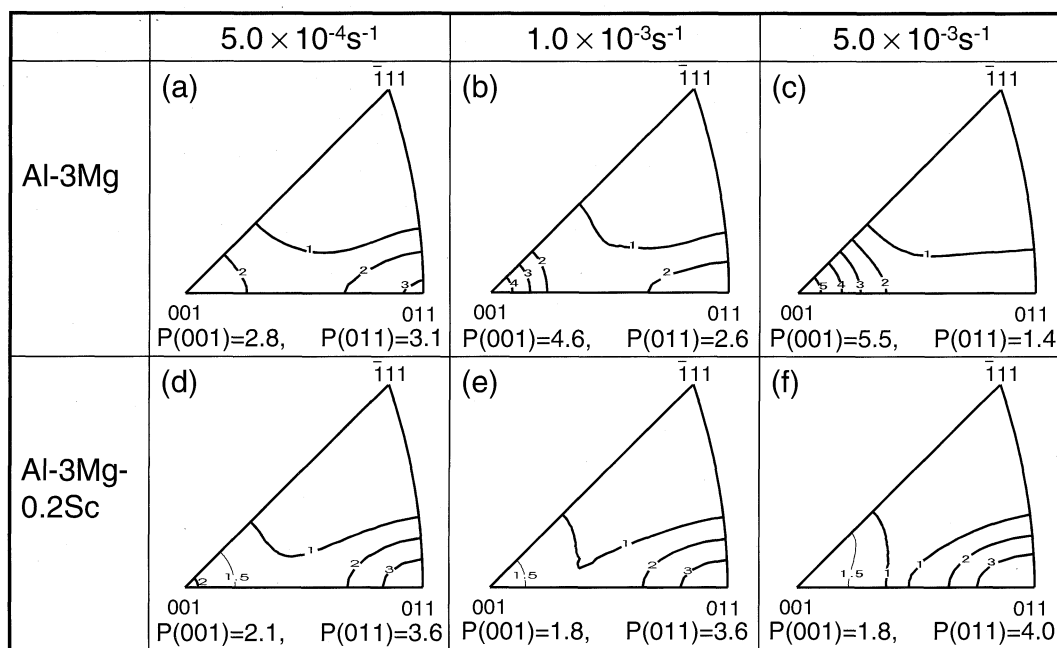


Fig. 4 Inverse pole figures for the specimens compressed at 723 K, up to a true strain of -1.0 under a final strain rate of $5.0 \times 10^{-4} \text{ s}^{-1}$, $1.0 \times 10^{-3} \text{ s}^{-1}$ and $5.0 \times 10^{-3} \text{ s}^{-1}$. (a)–(c) and (d)–(f) show the results of Al-3Mg and Al-3Mg-0.2Sc, respectively. The distributions of pole densities of the compression plane are given. The average density is used as units. The pole densities at (001) and (011) are given below the figures.

curves for Al-3Mg-0.2Sc are similar to that of Al-3Mg reported by the other researchers^{1,7)} as shown in Fig. 2. This indicates that the precipitates are coarse due to long time aging and hence their effect on the dislocation motion is quite limited.

3.3 Texture behaviors

The {111} pole figures are examined after the deformation at 723 K under a strain rate of $1.0 \times 10^{-3} \text{ s}^{-1}$ up to a true strain of -1.0 for Al-3Mg (Fig. 3(a)) and Al-3Mg-0.2Sc (Fig. 3(b)). Pole density is projected onto the compression plane. The average pole density is used as units. The pole density is distributed on latitude circle in both figures. This

means the formation of fiber textures in both alloys. In the present study, formation of fiber texture was confirmed for all of the deformation conditions by the examination on pole figures. In Fig. 3(a), the area of high pole density appears about 35° and 55° away from the center. In Fig. 3(b), the area of high pole density appears about 35° away from the center. The area of high pole density spreads to about 55° away from the center.

Figure 4 shows the inverse pole figures for the specimen deformed at 723 K up to a strain of -1.0 under strain rates of $5.0 \times 10^{-4} \text{ s}^{-1}$, $1.0 \times 10^{-3} \text{ s}^{-1}$ and $5.0 \times 10^{-3} \text{ s}^{-1}$. The results of Al-3Mg and Al-3Mg-0.2Sc are given in Figs. 4(a)–(c) and (d)–(f), respectively. Again, the average pole density

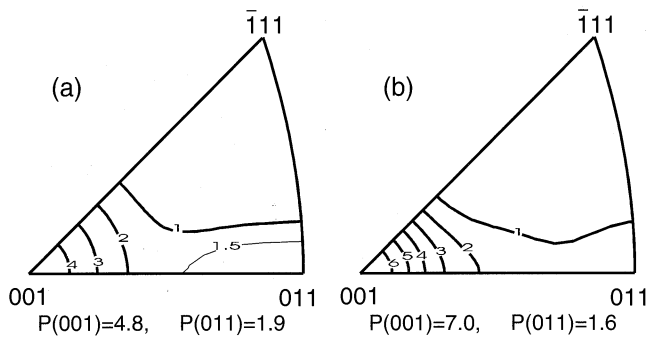


Fig. 5 Inverse pole figures for Al-3Mg compressed at 723 K, up to a true strain of -1.4 under final strain rates of (a) $5.0 \times 10^{-4} \text{ s}^{-1}$ and (b) $1.0 \times 10^{-3} \text{ s}^{-1}$.

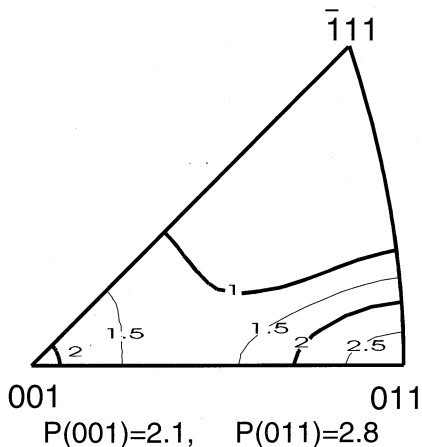


Fig. 6 Inverse pole figure for Al-3Mg-0.2Sc compressed at 723 K, up to a true strain of -1.5 under a final strain rate of $5.0 \times 10^{-4} \text{ s}^{-1}$.

is used as units for drawing the contour lines. Accumulation of pole density is observed at (001) and (011) in all of six inverse pole figures, namely $\{001\} + \{011\}$ double fiber texture is constructed irrespective of the kind of alloys and deformation conditions. However, difference in the effect of deformation condition on the texture development is observed between Al-3Mg and Al-3Mg-0.2Sc. Comparison of pole densities at (001) and (011) given below the figures suggests that development in $\{001\}$ component and weakening in $\{011\}$ component occur in the case of Al-3Mg as shown in Figs. 4(a)–(c), while no big change in the pole densities at (001) nor (011) exists between Figs. 4(d) and (f) for Al-3Mg-0.2Sc.

Figures 5(a) and (b) show the inverse pole figures for Al-3Mg compressed at 723 K up to true strains of -1.4 under a final strain rate of $5.0 \times 10^{-4} \text{ s}^{-1}$ and $1.0 \times 10^{-3} \text{ s}^{-1}$, respectively. With an increase in strain from -1.0 (Figs. 4(a) and (b)) to -1.4 (Figs. 5(a) and (b)), the pole intensity increases at (001) and decreases at (011); a sharp fiber texture with $\{001\}$ component is formed in Al-3Mg alloy. However, with an increase in strain from -1.0 (Fig. 4(d)) to -1.5 (Fig. 6) for Al-3Mg-0.2Sc alloy, weakening in $\{011\}$ component and no change in $\{001\}$ component are observed.

3.4 Grain structure after deformation

A part of the Grain structure maps derived from EBSD

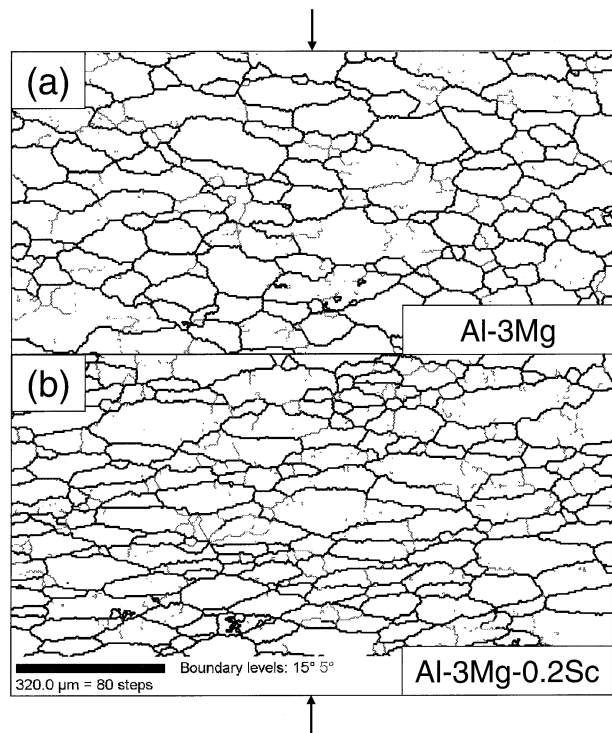


Fig. 7 Grain structure maps, derived from EBSD measurement, of (a) Al-3Mg and (b) Al-3Mg-0.2Sc compressed at 723 K under a final strain rate of $5.0 \times 10^{-4} \text{ s}^{-1}$ up to a true strain of -1.0 . The arrows indicate the compression axes.

measurements on the specimens deformed at 723 K are shown in Figs. 7 and 8. High angle grain boundaries are drawn by a misorientation angle greater than 15° using black thick lines. Low angle grain boundaries are drawn by a misorientation angle between 5° and 15° using gray thin lines. Figures 7(a) and (b) correspond to inverse pole figures shown in Figs. 4(a) and (d), respectively. The observations are conducted on the transverse section; the arrows in the figures indicate the compression axes. The mean grain aspect ratios (vertical length/horizontal length of the crystal grains) evaluated by linear intercept methods from these grain structure maps are about 0.7 and 0.3, respectively.

The grain structure maps for compression plane are shown on Al-3Mg (Fig. 8(a)) and Al-3Mg-0.2Sc (Fig. 8(b)) compressed at 723 K under a strain rate of $5.0 \times 10^{-4} \text{ s}^{-1}$ up to a strain of about -1.5 . There are a lot of grains with irregular shape in Fig. 8(a). The shape of the grains suggests that several subdivided grains combine to one big grain by grain boundary migration. A small number of the low angle grain boundaries exist in Fig. 8(a). In contrast, a large number of the low angle grain boundaries, and small grains exist around the big grains in Al-3Mg-0.2Sc alloy as shown in Fig. 8(b).

4. Discussion

4.1 Mechanism of high temperature deformation

In solid solution hardening type alloys, it is known that the dislocations can move with the Cottrell atmosphere in a certain range of high temperature deformation conditions:^{1,2)} so called atmosphere dragging becomes possible. Work softening is one of the indications of atmosphere dragging. It

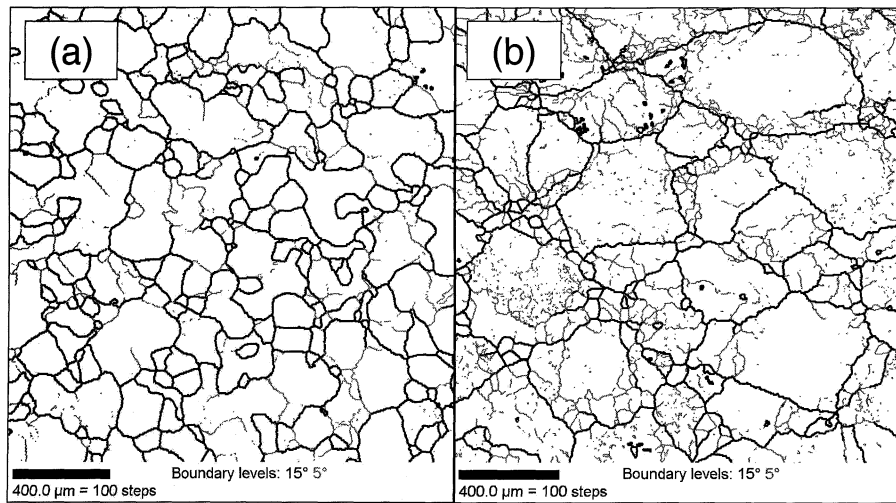


Fig. 8 Grain structure maps, derived from EBSD measurement, of (a) Al-3Mg and (b) Al-3Mg-0.2Sc compressed at 723 K under a strain rate of $5.0 \times 10^{-4} \text{ s}^{-1}$ up to a true strain of -1.4 and -1.5 , respectively.

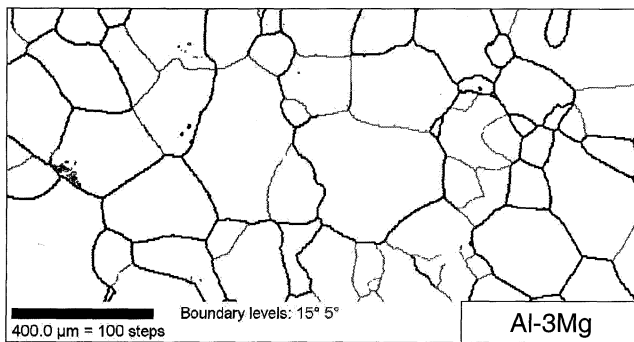


Fig. 9 Grain structure map, derived from EBSD measurement, of Al-3Mg compressed at 723 K up to a true strain of -0.1 under the same initial strain rate as in Fig. 4(b).

is understood that the dislocation velocity decreases around the yield point due to the multiplication of dislocations, resulting in the decrease in the flow stress. Although there are other possibilities causing work softening during high temperature deformation, such as dynamic recrystallization,⁸⁻¹⁰ adiabatic deformation¹¹) etc., atmosphere dragging is most plausible in the present case. In order to examine the occurrence of dynamic recrystallization, the compression test was conducted at 723 K up to a true strain of -0.1 close to the peak strain under the same initial strain rate as in Fig. 4(b), and microstructure was observed. Figure 9 shows the grain structure map after the deformation. No new grains are observed. This means that work softening can not be attributed to dynamic recrystallization.

Figure 10 is the double logarithmic plot showing the true stress vs. true strain rate relationship for the compression at 723 K. The true stress is evaluated at a true strain of -0.5 . The filled circles and the open circles show the results on Al-3Mg and Al-3Mg-0.2Sc, respectively. Both alloys fall on the same straight line. The stress exponent evaluated from the slope of the line is about 3. This coincides with the results reported by the other researchers.^{12,13}) Namely in these deformation conditions, it is considered that the deformation is controlled by the viscous motion of dislocations.^{2,12})

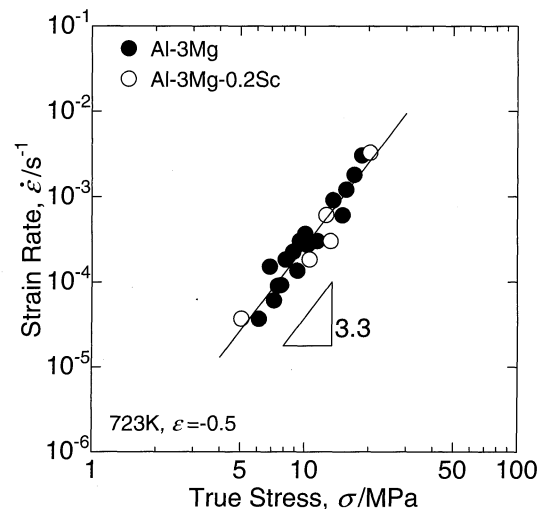


Fig. 10 True stress vs. true strain rate relationship compressed at 723 K. The filled circles and open circles show the results of Al-3Mg and Al-3Mg-0.2Sc, respectively.

The grain aspect ratio in Fig. 7(b) is about 0.3. The aspect ratio for the true strain of -1.0 derived from the geometrical evaluation under the constant volume assumption is 0.22; this suggests that the Al_3Sc precipitates effectively reduced the grain boundary migration. The stress levels for Al-3Mg-0.2Sc are almost the same as that of Al-3Mg. This indicates that the Al_3Sc precipitates produced by long time aging are not effective obstacles for dislocation motion.

4.2 Texture change

As shown in Figs. 4(a) and 5(a), the formation of $\{011\}$ texture of Al-3Mg alloy precedes the development of $\{001\}$ texture. The $\{001\}$ texture does not seem to be formed by continuous orientation change from the $\{011\}$ texture, because two independent density peaks are observed around (001) and (011) in inverse pole figure. The inverse pole figures of Al-3Mg-0.2Sc (Figs. 4(d)–(f)) show that the development of $\{001\}$ texture does not occur because of reducing grain boundary migration by Al_3Sc precipitates.

This means that {001} component of texture in Figs. 4(a)–(c) develops by consuming {011} and other grains. Inverse pole figures of Al-3Mg-0.2Sc with increase in strain from -1.0 (Fig. 4(d)) to -1.5 (Fig. 6) show the weakening in {011} textures. This suggests the occurrence of dynamic recrystallization during high temperature deformation. Figure 8(b) is also an evidence for dynamic recrystallization where a lot of small grains are observed around large grains.

4.3 Development mechanism of {001} texture

Otsuka and Horiuchi¹⁴) investigated the lattice rotation of Al-3 mol%Mg single crystals with various orientations by tensile creep tests where the viscous motion of dislocations dominates the deformation. The present authors³) also investigated lattice rotation of Al-3 mass%Mg single crystals by compression tests where the viscous motion of dislocation is the dominant deformation mechanism. The amount of lattice rotation was quite small when the initial orientations are close to (001), which coincides with the result by Otsuka and Horiuchi. These findings suggest that {001} orientation is stable for the uniaxial deformation. Weak but obvious peak in the pole density at (001) of Al-3Mg-0.2Sc appearing in Figs. 4(d) to (f) suggests that the grains with {001} orientations remained after the large amount of deformation due to their stability. Gourdet and Montheillet¹⁵) have been reported stability of {001} orientation as quasi-stable orientation using single crystals of AA1199 pure aluminum. They showed that a cubic sample of {001} orientation retained high pole density, at its original location after compression at 380°C to strain of -1.5 under strain rate of 10^{-2} s^{-1} . This is an evidence that {001} orientation is stable for the uniaxial deformation at high temperature.

In the case of the single crystals with initial orientations far from {001}, the amount of lattice rotation was larger than that for the orientations close to {001}. The direction of the lattice rotation coincided with the expectation based on the single slip of {111}⟨110⟩ system.³)

Development of {011} texture is also found on Al-3Mg-0.2Sc as shown in Figs. 4(d)–(f). This indicates that the formation of {011} fiber texture can be attributed to the slip deformation by {111}⟨011⟩ slip. It is thus concluded that the texture change in Al-3Mg from {011} + {001} to {001} textures is caused by grain boundary migration which extends the grains with {001} orientation.

5. Conclusions

In order to understand the formation mechanism of {001}

fiber texture during the high temperature uniaxial compression deformation of Al-3 mass%Mg solid solution alloy, deformation and texture development behaviors of Al-3Mg and Al-3Mg-0.2Sc alloys were investigated under various temperatures and strain rates up to various amounts of true strain. It has been found that fiber texture is constructed in all the deformation conditions. Increase in strain rates results in the change in the main component of the fiber texture for Al-3Mg, while no obvious change in the main component is observed in the case of Al-3Mg-0.2Sc. That is, the transition from {001} + {011} fiber texture to {001} fiber texture is strongly suppressed by Al₃Sc precipitates. It is thus concluded that development of the {001} texture is attributable to the growth of {001} oriented grains by grain boundary migration.

Acknowledgements

The authors thank Ms. H. Shimada, graduate student of Yokohama National University, for her assistance in conducting experiments. The authors also appreciate to The Japan Light Metal Educational Foundation, Inc. for the financial support.

REFERENCES

- 1) R. Horiuchi, H. Yoshinaga and S. Hama: *Trans. Japan Inst. Metals* **6** (1965) 123–130.
- 2) A. H. Cottrell and M. A. Jaswon: *Proc. R. Soc. A* **199** (1949) 104–114.
- 3) K. Okayasu and H. Fukutomi: *Mater. Sci. Forum* **495–497** (2005) 579–584.
- 4) K. Okayasu and H. Fukutomi: *J. Japan Inst. Metals* **70** (2006) 562–567.
- 5) M. Dahms and H. J. Bunge: *J. Appl. Cryst.* **22** (1989) 439–447.
- 6) K. Ihara and Y. Miura: *Mater. Sci. Eng. A* **387–389** (2004) 647–650.
- 7) S. R. Chen and U. F. Kocks: *Hot Deformation of Aluminum Alloys*, ed. by T. G. Langdon, H. D. Merchant, J. G. Morris and M. A. Zaidi, (The Minerals, Metals and Materials Society, 1991) pp. 89–104.
- 8) M. J. Luton and M. Sellars: *Acta Metall.* **17** (1969) 1033–1043.
- 9) T. Sakai and J. J. Jonas: *Acta Metall.* **32** (1984) 189–209.
- 10) M. Hasegawa and H. Fukutomi: *Acta Mater.* **51** (2003) 3939–3950.
- 11) Y. B. Guo, Q. Wen and M. F. Horstemeyer: *Int. J. Mech. Sci.* **47** (2005) 1423–1441.
- 12) R. Horiuchi and M. Otsuka: *Trans. Japan Inst. Metals* **13** (1972) 284–293.
- 13) H. Oikawa, K. Honda and S. Ito: *Mater. Sci. Eng.* **64** (1984) 237–245.
- 14) M. Otsuka and R. Horiuchi: *J. Japan Inst. Metals* **36** (1972) 809–817.
- 15) S. Gourdet and F. Montheillet: *Mater. Sci. Eng. A* **283** (2000) 274–288.